Surface Immobilisation of Transition Metal Substituted Krebs Type Polyoxometalates, $[X_2W_{20}M_2O_{70}(H_2O)_6]^{n-}$ (X = Bi or Sb, M = Co^{2+} or Cu^{2+}), by the Layer by Layer Technique

Aidan Fagan Murphy[1] and Timothy McCormac[2]*

[1] Department of Applied Science

Institute of Technology Tallaght

Tallaght, Dublin 24

Ireland

[2] Electrochemistry Research Group

Dundalk Institute of Technology

Department of Applied Science

Dundalk, County Louth

Ireland

*Corresponding author; tim.mccormac@dkit.ie

Tel: +353-42-9370459

Fax: +353-42-9331163

Abstract

A series of transition metal (i.e. Cu^{2+} and Co^{2+}) substituted Krebs type Polyoxometalates (POMs), of the general formula $[X_2W_{20}M_2O_{70}(H_2O)_6]^{n-}$, X = Sb or Bi, M = Co(II) or Cu(II), have been successfully immobilised onto carbon electrode surfaces through the employment of the layer-by-layer (LBL) technique. This involved the construction of alternating anionic POM, $[X_2W_{20}M_2O_{70}(H_2O)_6]^{n-}$, layers and the cationic metallodendrimer, Ru(II)-metallodendrimer as the cationic layers, in addition to a [poly(diallyldimethylammonium chloride)] PDDA base layer. Stable multielectron redox couples associated with the W-O framework, for the Krebs type POMs, and the Ru(III/II) for the metallodendrimer, were clearly observed upon layer construction and redox switching within the pH domain of 2 to 6.5. The constructed multilayer assemblies exhibited pH dependent redox activity and thin layer behaviour up to 100 mV s^{-1}. The porosity and permeability of the individual multilayer assemblies towards an anionic probe was determined by AC impedance and cyclic voltammetry. The surface morphology of each multilayer was also determined by Atomic Force Microscopy (AFM).

Keywords: *Polyoxometalate; Krebs; Immobilisation; Layer by Layer (LBL);*

1. Introduction

Polyoxometalates (POMs) are a class of redox active compounds formed from metal oxide subunits possessing discrete and varied redox chemistry that typically occurs with little to no change in the structure of the molecule. The varied and extensive properties of different polyoxometalates, such as their electrical, magnetic, optical and structural properties, has lead to them being employed across a wide range of applications, from catalysis to electronic devices [1-14]. The Krebs-type polyoxometalates, $[X_2W_{20}M_2O_{70}(H_2O)_6]$, X = heteroatom, M = transition metal, are a sandwich type of polyoxometalates containing two transition metals between two $[XW_9O_{33}]$ fragments as described in [15, 16]. This work focuses on the Krebs-type polyoxometalates $[Bi_2W_{20}Co_2O_{70}(H_2O)_6]^{10-}$, $[Sb_2W_{20}Co_2O_{70}(H_2O)_6]^{10-}$ and $[Sb_2W_{20}Cu_2O_{70}(H_2O)_6]^{8-}$, referred to hereafter through their heteroatom and transition metal, i.e. $[BiCo]^{10-}$, $[SbCo]^{10-}$ and $[SbCu]^{8-}$, respectively. These polyoxometalates have been previously synthesised in [15, 16] but had not been explored in any significant detail.

In order to reliably produce polyoxometalate-based devices for specific purposes a reproducible and practical method for their construction must be considered. Several methods are possible, including polymer doping and electrodeposition [17-30], the method utilised here is the layer-by-layer method. This layer-by-layer method has been known significant and reproducible film growth for a variety of applications while remaining a simple and rapid method for film formation [31 - 35]. The layer-by-layer method uses alternating layer of cationic and anionic species in succession to form a multi-layer film on the desired surface. Such layer are formed from solution by electrostatic attractive of solution species to the film surface. This is repeated by exposure

of the film to different solutions containing either the cationic or anionic species to be adhered in repetition in order to construct the film.

This work examines the properties of these polyoxometalates, $[BiCo]^{10-}$, $[SbCo]^{10-}$ and $[SbCu]^{8-}$, when contained with a multi-layered film composed of a base PDDA (polydiallydimethylammmonium) cationic layer followed by alternating layer of the anionic polyoxometalate and cationic ruthenium (II) pentaerythritol based metallodendrimers (ruthenium metallodrimer). The electrochemical behaviour of each polyoxometalates and the possibility of copper expulsion from the tungsten-oxide framework is examined. The structure of these films and its influence on their displayed properties is further examined by comparison to the behaviour of a well-known redox couple, potassium ferri/ferrocyanide, at potential inactive regions for the polyoxometalate-based film, as the film is constructed. This gave greater insight into additional physical/structural considerations for the film based properties involving solution based species.

2. Experimental

2.1 Materials

All starting materials were of synthetic grade and purchased from Sigma-Aldrich and unless stated otherwise they were used as received. Synthesis of the desired polyoxometalates followed established literature procedures [15, 16]. Ruthenium metallodendrimer was prepared as described in the literature [36]. Electrolytes were prepared using synthetic grade starting compounds purchased from Sigma-Aldrich.

2.2 Apparatus and Procedures

All electrochemical experiments were performed using a single compartment three electrode electrochemical cell. A glassy carbon working electrode (0.0707 cm^2), platinum counter electrode and silver/silver chloride (3M KCl) reference electrode were used for all electrochemical measurements unless stated otherwise. The working electrode was polished using 1.0, 0.3 and 0.05 micron alumina powder for two minutes each in succession and rinsed with deionised water prior to further use. Electrochemical experiments were performed with different CHI electrochemical instruments. These are CHI660A, CHI420a or CHI660c potentiostats. Electrolytes used included 0.5 M Na_2SO_4 and 0.5 M CH_3COONa, over the pH range 1.00 to 3.50 and pH 4.00 to 6.50 with pH adjustment with 0.5 M H_2SO_4 or CH_3COOH respectively. Alternating Current (AC) impedance studies were performed in a 0.1 mM potassium ferricyanide, 0.1 mM potassium ferrocyanide with 0.1M potassium chloride as the electrolyte solution. Kinetic studies examining the variance in the standard rate constant (k^0) of potassium ferricyanide with the build-up of layers at the electrode surface were performed in 1 mM potassium ferricyanide with 0.1 M potassium sulphate as the electrolyte solution.

2.2.1 Multilayer Construction

The formation of multiple adhered layers was achieved using the layer-by-layer method previously described in the literature [37, 38]. The three solutions employed were; 8% (v/v) PDDA (poly(diallydimethylammonium chloride)) in HPLC grade water, 2.0 mM of the desired polyoxometalate in HPLC grade water and 0.2 mM ruthenium metallodendrimer in acetonitrile. Construction of the film was performed as follows: A

glassy carbon electrode was polished with 1.0, 0.5 and 0.03 µm alumina powder in succession for approximately ten minutes. The electrode surface was then roughened with 0.5 µm for four minutes. (1) This electrode was immersed in 8% PDDA solution for one hour. The electrode was then rinsed in HPLC grade water for five minutes before gently drying with argon gas. (2) The electrode was then immersed in a 2.0 mM polyoxometalate solution for thirty minutes. After this the electrode was rinsed in HPLC grade water for five minutes before drying with argon gas. (3) The electrode was then immersed in 0.2 mM ruthenium metallodendrimer solution for twenty minutes. The electrode was then dried with argon gas. Steps (2) and (3) were repeated a total of five times resulting in a total of six bi-layers consisting of one underlying PDDA layer, five ruthenium metallodendrimer layers and six polyoxometalate layers, typically with an outer POM layer. The formation of these assemblies was monitored by cyclic voltammetry. After the deposition of each polyoxometalate layer the electrode was rinsed in HPLC grade water for five minutes and then placed in pH 2.0, 0.5 M Na_2SO_4 electrolyte and the applied potential was cycled over the redox activity of the polyoxometalate tungsten-oxide framework.

2.2.2 AC Impedance Measurements

AC impedance studies were performed by placing the modified POM Multilayer electrodes in a 0.1M KCl solution of 0.1 mM $K_3Fe(III)(CN)_6$ / $K_4Fe(II)(CN)_6$ with the application of +223 mV (versus Ag/AgCl) from 0.1 to $1x10^6$ Hz and with a voltage amplitude of 5 mV. The electrolyte was prepared fresh before use. During the experiment the electrolyte was stored in the dark and constantly degassed for the extent of each experiment.

2.2.3 Heterogeneous Kinetic Investigations

After the deposition of each layer the modified electrode was placed in a solution of 1 mM potassium ferricyanide with 0.1 M K_2SO_4 and cyclic voltammetry performed over the ferri/ferrocyanide redox couple, at scan rates between 5-700 mVs^{-1}. After this the electrode was rinsed in HPLC grade water for five minutes and dried with argon gas. Then the formation of the film was continued as described previously with examination of potassium ferricyanides k^0, standard rate constant, value after the deposition of each layer. The modified electrode was rinsed after the deposition of each step prior to these voltammograms as during its construction. These studies were performed in 0.1 M K_2SO_4.

3. Results and Discussion

The main aim of this paper is to investigate the possibility of surface immobilising a variety of transition metal (i.e. Cu(II), Co(II)) Krebs type polyoxometalates onto glassy carbon surfaces through application of the layer-by-layer (LBL) technique. The resulting electrochemical and surface properties of the POM based multilayers were then elucidated. However it is important firstly to give a brief overview of the solution electrochemistry of each of the Krebs type POMs employed in this study. The detailed study of their solution redox properties along with their electrocatalytic properties will be the subject of a future paper.

3.1 Solution Redox Properties $[X_2W_{20}M_2O_{70}(H_2O)_6]^{n-}$ (X = Bi, Sb, M = Co^{2+}, Cu^{2+})

The basic cyclic voltammograms for each of the $[X_2W_{20}M_2O_{70}(H_2O)_6]^{n-}$ (X = Sb or Bi, M = Co^{2+} or Cu^{2+} n = 10^- or 8^-) polyoxometalates and their precusors are displayed in Figure 1 A-F. Each polyoxometalate displayed a multiple four electron reduction process, the

number of electrons transferred being confirmed by use of an internal standard, with $E_{1/2}$ values of -467 mV, -517 mV, -461 mV and -452 mV (versus Ag/AgCl), for $[BiCo]^{10-}$, $[BiCu]^{8-}$, $[SbCo]^{10-}$ and $[SbCu]^{8-}$, respectively at pH 2.5. This corresponds to the redox activity associated with each of the polyoxometalates' tungsten-oxo frameworks. The polyoxometalates that contain copper showed additional redox activity between -200 to 200 mV associated with the Cu^{2+}/Cu^{0} redox couple. The copper redox activity indicated adsorption and desorption processes from the electrode surface upon its reduction and oxidation, respectively. It is well known in the literature that the reduction of polyoxometalate's tungsten-oxide framework is accompanied by protonation countering the polyoxometalates' increased negative charge. This is the case for the Krebs type polyoxometalates investigated here. In general the tungsten-oxo redox activity for each of the polyoxometalates shifted to more negative potentials in more alkaline pHs with some dependence as well upon the nature of the electrolyte. The number of H^{+} ions involved in the redox couples for each polyoxometalate can be calculated by employment of equation 1 below:

$$\frac{dE}{dpH} = -59.1\frac{m}{n}mVpH^{-1} \qquad \text{eqn. 1}$$

where m is the number of protons and n is the number of electrons involved in the redox process. In general for the first four electron redox process associated with the Co(II) Krebs type POMs equation 2 below shows the role of the added protons in the redox process

$$[Sb_2W_{20}Co_2O_{70}]^{10-} + xH^{+} + 4e^{-} \leftrightarrow H_x[Sb_2W_{20}Co_2O_{70}]^{(10+4-x)-} \qquad \text{eqn. 2}$$

The number of protons involved in the tungsten-oxo redox process for each POM was 7 and 5 for the pH ranges 1 to 3.5 and 4 to 6.5, respectively. Previously [39], the Fe(III) form of the Krebs POM, $[SbFe]^{8-}$, displayed a pH sensitivity of 89 $mVpH^{-1}$ from pH 1 to pH 7 in the same electrolyte, 0.5 M Na_2SO_4 adjusted with 0.5 M H_2SO_4 and 0.5 M CH_3COONa adjusted with CH_3COOH.

3.2 Multilayer Films

3.2.1 Basic Redox Properties

Attempts to grow the Krebs polyoxometalate based multilayers by either employing PDDA or the ruthenium metallodendrimer as the cationic moiety within the multilayer assembly was investigated. However the majority of the assemblies formed with PDDA as the cationic layer displayed limited and random film growth and as a result PDDA / Krebs based assemblies were not investigated further in any detail. In contrast, assemblies constructed with the $[BiCo]^{10-}$, $[SbCo]^{10-}$ and $[SbCu]^{8-}$ Krebs polyoxometalate anionic layers with an initial PDDA layer and subsequent ruthenium metallodendrimer cationic layers all displayed continuous layer growth. However attempts to form multilayers with the $[BiCu]^{8-}$ polyoxometalate proved unsuccessful and hence these films are not discussed further. As has been previously suggested in the literature [31], the close matching between the polyoxometalate's anionic charge and that of the ruthenium metallodendrimer is the likely reason why the assemblies composed with the latter cationic moiety resulted in more stable film growths as compared to films composed of PDDA. For each of the polyoxometalate-based films the ruthenium metallodendrimer

displayed a redox couple, Ru^{3+}/Ru^{2+}, with an $E_{1/2}$ of +1.05V V (vs Ag/AgCl), which was independent of solution pH.

$[XCo]^{10-}$-based films (where X is Bi or Sb)

The continuous growth of $[BiCo]^{10-}$ based films is shown in Figure 2(a). Film construction was performed several times, each showed a general increase in the POM's tungsten-oxide peak currents with increasing layer number. The oxidation peak current growth was much more distinct and linear with layer number than that of the reduction peak current. After deposition of six bi-layers a four electron redox couple with an $E_{1/2}$ = ~ -440 mV at pH 2.0 was observed in the same general potential region as that of the polyoxometalate's tungsten-oxide framework redox activity in solution. Surface coverage was calculated from equation 3 below:

$$Q = nFA\Gamma \qquad \text{eqn. 3}$$

Where Q is the charge passed, n is the number of electrons involved in the redox process, being 4 in this case, F is Faraday's constant (96,485 $Cmol^{-1}$), A is the electrode's surface area (0.0707cm^2) and Γ is the surface coverage (mol cm^{-2}). Figure 2(b) displays the variation in the surface coverage with the layer number based on the reduction peak of W1. A general increase in the polyoxometalate concentration can be seen up to six bi-layers. Some variation in the overall film growth occurred between repetitions. This has been attributed to manual roughening of the underlying electrode surface, prior to film formation.

Figure 3(a) displays the shift in the tungsten-oxide redox process for the $[BiCo]^{10-}$-based multi-layer as a function of solution pH. The four electron W1 redox process of $[BiCo]^{10-}$ present in the film was pH sensitive with its $E_{1/2}$ displaying pH dependence of 75.6 and 74.9 $mVpH^{-1}$ over the pH ranges 1.0-3.5 and 4.0-6.5, respectively, as seen in Figure 3(b). From the slopes of the plots in figure 3(b) a total of five H^+ for both pH ranges are involved in the redox process W1. For the pH range 1.0-3.5 slight differences in the E_{pc} and E_{pa} pH dependence, 71.4 and 79.8 $mVpH^{-1}$ respectively, result in decreasing peak separation with increasing pH. Over the 4.0-6.5 pH range the pH sensitivities of E_{pc} and E_{pa}, 74.9 mV and 75.0 mV pH^{-1} respectively, were nearly identical resulting in little change in peak separation over this pH range. A scan rate study was performed upon the $[BiCo]^{10-}$-based film between the scan rates 10mV to 3000mV s^{-1}. As can be seen in Figure 4(b), the $[BiCo]^{10-}$ film exhibited thin layer behaviour up to 100mV s^{-1}.

The antimony analogue of the Co(II) Krebs, $[SbCo]^{10-}$, showed very similar behaviour to it's bismuth analogue, except that two tungsten-oxo redox couples were observed during film growth. The first redox couple occurred at more positive potentials, $E_{1/2}$ = ~ -456 mV, labelled W1, and was approximately two to three times the intensity of the second redox couple, $E_{1/2}$ = ~ - 558 mV. A general increase in the surface coverage with layer number was observed with a measured surface coverage of 6.5 x 10^{-11} $molcm^{-2}$ after the deposition of 6 bilayers. The W2 process over the pH range 1.0-3.0 exhibited a pH dependence for its E_{pc}, E_{pa} and $E_{1/2}$ of 78.0, 79.0 and 78.5 $mVpH^{-1}$, respectively. W2 however was not observed outside these pH values. W1 displayed slightly different pH dependence for the two different pH ranges. The pH dependence of W1's $E_{1/2}$ was

observed as 71.0 and 73.5 $mVpH^{-1}$ over the pH ranges 1.0-3.5 and 4.0-6.5, respectively. Slight differences in W1's E_{pc} and E_{pa} pH dependence over the pH range 1.0-3.5 resulted in decreased peak separation with increased pH. Over the pH range 4.0-6.5 both E_{pc} and E_{pa} have almost identical pH dependence. Taking W1 as a four electron process and using equation 1 gave five H^+ ions involved in this redox process over both pH ranges examined. In comparison, the W1 redox couple of $[SbCo]^{10-}$ in solution involved seven and five electrons for the pH ranges 1.0-3.5 and 4.0-6.5, respectively. In addition the $[SbCo]^{10-}$ multilayer exhibited thin layer behaviour up to $100mVs^{-1}$ as seen with the $[BiCo]^{10-}$ mutilayer.

$[SbCu]^{8-}$-based films

As described in section 3.1 the $[SbCu]^{8-}$ POM exhibits redox activity associated with it's Cu(II) centre and tungsten-oxo framework. Figure 5 shows the resulting cyclic voltammograms obtained during the formation of the $[SbCu]^{8-}$-based films. What is immediately apparent is that these films display more complicated redox activity than either the $[BiCo]^{10-}$ or $[SbCo]^{10-}$ POMs previously discussed. A redox couple with an $E_{1/2}$ of approximately -100 mV only occurred in the initial bi-layer, which is believed to be due to the redox switching of the POM's Cu(II) centre. Three redox processes followed with $E_{1/2}$'s of ~ -352 mV, -441 mV and -564 mV, labelled W1-W3 respectively were also observed during film growth with the appearance of an additional reduction peak at -288 mV, labelled W4, being observed during film growth. As with the other layers the oxidation peak currents increased with layer number while more variation was observed for the reduction peak currents. Calculation of the surface coverages for the film proved

difficult due to the uncertainty in the number of electrons involved in each of the observed redox processes, W1 to W3. The apparent loss of electroactivity for the Cu(II) centre upon layer growth suggested possible copper removal from the POM during film growth. Multilayer films composed of $[Sb_2W_{22}O_{74}(OH)_2]^{12-}$ and the ruthenium metallodendrimer were hence grown and the resulting cyclic voltammograms obtained during the growth phase are shown in Figure 6 . Following the deposition of six bi-layers the $[Sb_2W_{22}O_{74}(OH)_2]^{12-}$-based films displayed three redox couples associated with the redox activity of the tungsten – oxo framework with $E_{1/2}$ values of ~ -300 mV, -458 mV and -566 mV, versus Ag/AgCl, labelled W1-W3. It can be seen that the position of these three redox peaks are in close agreement to those obtained for the $[SbCu]^{8-}$ films shown in Figure 5. These results indicate that upon film formation there appears to be a partial removal of the Cu(II) centre from the polyoxometallate's cage. Recently [40] films based on transition metal substituted sandwich-type polyoxometalates focused on the fate of the transition metal after immobilisation. The addition of the transition metal and its variation in size and charge in comparison to the metal oxide unit it was replacing were suspected of leading to more fragile polyoxometalate structures, noted for the Wells-Dawson type polyoxometalates, α_1-$[P_2W_{17}V^{VI}O_{62}]^{8-}$ and α_2-$[P_2W_{17}O_{61}(OH)_2Fe^{III}]$ [40]. Electrostatic repulsion from the cationic film layer was suggested in the literature as the probable cause for the partial or complete ejection of the transition metals from the polyoxometalate structure [40]. This ejection was observed by the loss of the transition metal's redox activity within the film [40]. The formation of the lacunary polyoxometalate by transition metal expulsion was confirmed by comparison to a film formed separately with the prepared lacunary polyoxometalate [40]. Minor responses in

the region of the transition metal's redox activity, typically not capable of being observed when the polyoxometalate's metal-oxide framework was also examined, suggested that any degradation/metal ejection was incomplete [40].

Interestingly when $[SbCu]^{8-}$ films were constructed with PDDA as the cationic moiety the resulting films displayed the continued presence of minor copper oxidation activity, which indicated that the polyoxometalate had not been completely degraded. The loss of the copper redox activity, the similarities to films formed with $[Sb_2W_{22}O_{74}(OH)_2]^{12-}$ and the presence of minor redox activity observed at the expected potentials for Cu(II)/Cu(0) activity suggested that $[SbCu]^{8-}$ has been partly converted to the lacunary analogue. In the literature [39], partial preservation of the transition metal substituted polyoxometalate structure occurred but only displayed minor redox activity as it was overshadowed by the activity of the metal-oxide framework. This was also observed here for these $[SbCu]^{8-}$ based films indicating that these films were composed of a mixture of the lacunary and metal substituted polyoxometalate. The difference observed between the films constructed with PDDA and the Ruthenium metallodendrimer in terms of the fate of the Cu(II) centre is probably due to the higher positive charge of +8 on the ruthenium metallodendrimer thereby resulting in stronger electrostatic repulsion effects.

For the $[SbCu]^{8-}$ films the redox processes W1, W2 and W3 displayed $E_{1/2}$ pH dependencies of 63.2, 73.2 and 70.9 $mVpH^{-1}$ over the pH range 1.0-3.5 and 31.8, 75.4 and 78.7 $mVpH^{-1}$ over the pH range 4.0-6.5, respectively. W2 and W3 displayed similar pH dependencies to each other, which were lower than the polyoxometalate's single four

electron redox couple in solution. There was also less variation between their E_{pc} and E_{pa} pH dependence for both pH ranges. W1 behaves significantly differently to W2 or W3, over the pH range 1.0-3.5 W1 possesses slightly lower pH dependence then either W2 or W3. For the pH range 4.0-6.5 0.5 M CH_3COONa W1 is approximately half as sensitive to pH as W2 or W3. Due to the uncertainties in the number of electrons associated with each of the individual redox processes W1 to W3, the number of protons transferred for each redox step could not be ascertained. In addition, for the $[SbCu]^{8-}$-based films, the close proximity and increased tailing of the three redox couples prevented accurate determination of their peak currents. At increased scan rates the redox responses for $[SbCu]^{8-}$-based films were nearly indistinguishable as individual processes.

Overall in terms of the pH studies for each POM based multilayer the individual polyoxometalate's redox response within the film remained sensitive to solution pH. Previously in the literature, Bi *et al.* [39] had shown that $[Sb_2W_{20}Fe_2(H_2O)_6]^{8-}$ was formed into a multi-layer film composed of alternating layers of this polyoxometalate and PDDA. This displayed a pH dependence in its four electron tungsten-oxide framework's redox activity of 74 $mVpH^{-1}$, over the pH range 1.0-7.0 in the same electrolytes used here. This pH dependence was similar that which was observed here for $[BiCo]^{10-}$, $[SbCo]^{10-}$ and $[SbCu]^{8-}$-based films. Previously in the literature [39], the four electron tungsten-oxide redox couple of multi-layer films composed of $[Sb_2W_{20}Fe_2(H_2O)_6]^{8-}$ and PDDA involved five protons, less then its solution behaviour which involved six protons. This was similar to that observed here for the $[BiCo]^{10-}$ and $[SbCo]^{10-}$-based films.

3.2.2 Atomic Force Microscopy (AFM) studies

AFM scans were performed over 5 and 20 μm^2 areas of ITO slides modified with the various polyoxometalate-based films, with an example of an AFM image for the $[SbCo]^{10-}$ film being given in Figure 7. As expected, the overall surface structure was heterogeneous in nature with significant variation in its characteristics over the entire film surface. Table 1 lists the R_a, average roughness, s, mean spacing between peaks, and R_p, maximum peak height, for the various polyoxometalate-based films The overall R_a, s and R_p values for the 20 μm^2 area are shown as well as those for smaller 5 μm^2 areas in Table 1 which served to highlight the variation that was present over the film surface. Films formed with $[BiCo]^{10-}$ or $[SbCu]^{8-}$ exhibited similar values for their surface roughness as well as for their peak spacing and maximum peak heights. Films formed with $[SbCo]^{10-}$ displayed lower surface roughness, reduced peak separation and peak height.

In comparison to the literature, films formed with $[Eu(SiW_{10}VO_{39})_2]^{15-}$ and polyethyleneimine [41] by the layer-by-layer method, built on a quartz slide, had a surface roughness of 2.4 nm, much less than for the films formed here, with even distribution across the sample surface. Fluorine doped transparent conductive tin oxide thin films, deposited by chemical vapour deposition, chemical spray pyrolysis or spray pyrolysis onto heated substrates using infra red irradiation [30], displayed surface roughness values between 5-35 nm, these values are similar to those observed for the $[X_2W_{20}M_2O_{70}(H_2O)_6]^{n-}$-based films formed here. Poly(ethylenimine), PEI and $BW_{12}O_{40}{}^{4-}$ Keggin structure polyoxometalate were formed as films on quartz slides and their growth by LBL monitored by AFM [42]. Initially for the 1st PEI/polyoxometalate bi-layer the surface roughness was 0.685 nm increasing to 1.115 nm by the 4th bi-layer and 1.330 nm

by the 8th bi-layer, the mean height also increased from 12.0 nm to 15.0 nm from the 4th to 8th bi-layer respectively. The film was observed to be initially heterogeneous with sub-monolayer coverage but increasing the number of deposited layers decreased these film defects [42]. In contrast to this literature, the polyoxometalate-based films formed here had much greater maximum peak heights with increased surface roughness which could be due to the underlying ITO surface. Overall these films were considered quite heterogeneous in their surface structure.

3.2.3 AC Impedance Studies

Figure 8 shows the real and imaginary, Z_{Re} and Z_{Im} impedances, respectively, of the ferri/ferrocyanide redox couple, at the bare electrode and at various stages of film layer deposition for a [BiCo]$^{10-}$ multilayer system with the arc and linear regions representing the kinetic and mass transfer controlled regions, respectively. As the film was grown the region under kinetic control increased in size with an associated increase in R_{ct}. The cross-over frequency between the two regions changed from approximately 550 Hz to 10 Hz for the bare and 7th film layer, respectively. Minor variations in the solution resistance, R_{Ω}, were noted between approximately 85-95 Ω. R_{ct} and i_0 values are given in Table 2 with the i_0 values being calculated from equation 4 below [43]:

$$R_{ct} = \frac{RT}{Fi_0} \qquad \text{eqn.4}$$

where R is the gas constant, T is temperature, i_0 is the exchange current and F is Faraday's constant. As can be seen R_{ct} values increased from approximately 75-790 Ω and i_0 values varied from 0.34 to 0.035 mA from the bare electrode to the 7th deposited layer. For the 3-7th layers, with ruthenium metallodendrimer as the outer layers, lower R_{ct}

values than expected were observed. Additionally, the simple equivalent circuit model used to derive these R_{ct} values predicts that each graph of Z_{Im} versus Z_{Re} for the various stages of film growth should possess a slope of unity at the low frequency limit, where it was under mass transport control. Generally this slope was found to decrease away from unity with increased film growth. The decrease in the low frequency Z_{Im} versus Z_{Re} slope with increasing layer number could be attributed to additional electronic components that occurred with film growth not accounted for in the original equivalent circuit model.

In summary the AC impedance results, as shown in Table 2, obtained for the polyoxometallate films displayed an increase in R_{ct} upon layer growth with a corresponding decrease in i_0. This increase in R_{ct}, as described in the literature for other systems [44], represented the reduced number of pathways and increased pathway length to the electrode surface for the redox probe upon layer build-up. The $[SbCu]^{8-}$-based film displayed a charge transfer resistance an order of magnitude higher than those of $[BiCo]^{10-}$ or $[SbCo]^{10-}$, with a much more significant kinetically controlled region, thereby indicating that the $[SbCu]^{8-}$-based film was less porous in nature. Some variation between the ruthenium metallodendrimer and polyoxometalate layers was noted for the cobalt POM variants with the outer ruthenium metallodendrimer layers possessing a lower than expected charge transfer resistance. No such behaviour was noted for the $[SbCu]^{8-}$-based film. Similar studies in the literature on PAH/PSS films, poly(allylamine hydrochloride) and poly(styrenesulfonate) respectively, formed on gold electrodes displayed R_{ct} values for potassium ferricyanide varying from 2-7, 10-20 to 5000 Qcm^2 for the 1^{st}, 2^{nd} and 3^{rd} bi-layers respectively [44]. Varying the pH of the electrolyte was

observed to cause swelling of the films of up to 40% over time which increased the films permeability at pH 10 with only minor changes at pH 3.2 and 6.3 for this film. The non-linear increase in R_{ct} from the 1st and 2nd bi-layers to the 3rd, 4th and 5th had been attributed to differences in film structure between the inner and outer layers. In contrast to this, $[BiCo]^{10-}$ and $[SbCo]^{10-}$-based films displayed a much more linear increase in R_{ct} with layer number, suggesting that the basic film structure remains the same as the film is constructed. Overall, films formed with $[SbCu]^{8-}$ can be considered much less porous than those formed with $[BiCo]^{10-}$ or $[SbCo]^{10-}$ with the cobalt variants being considered to be almost equivalent.

3.2.4 Heterogeneous Kinetic investigations

Reversible redox processes display a dependence on the redox active species' mass transfer to the electrode surface. They do not exhibit kinetic limitations on their response but can behave in a quasi-reversible or irreversible manner under certain conditions. This behaviour can be promoted by increasing the applied scan rate, ν. By observing the general properties of the system, such as peak height, shape, symmetry and separation, changing from reversible to quasi-reversible/irreversible with increasing scan rate it is therefore possible to deduce the system's standard rate constant for the electron transfer, k^0, as described in the literature for other systems [45, 46]. The redox behaviour of the well known model monoelectronic redox system, $Fe(CN)_6^{3-}/Fe(CN_6)^{4-}$ was investigated at the Krebs type polyoxometalate multilayer assemblies. The redox activity of the $Fe(CN)_6^{3-}/Fe(CN_6)^{4-}$ system occurred at potentials where the POM multilayers were redox inactive, thereby ensuring that the films behaved as unreactive structural features

on the electrode. The diffusion of the $K_3Fe(CN)_6$ to the underlying electrode occurred through the film and reflected the film's porosity, which includes film defects, pinholes and other physical features. After each layer was formed the redox behaviour of the $Fe(CN)_6^{3-}/Fe(CN_6)^{4-}$ system was investigated over a range of scan rates with the it's associated heterogeneous rate constant being measured through calculation of the peak to peak separation (ΔEp) by equation 5 [45, 46]:

$$\Psi = \frac{\left(\frac{D_O}{D_R}\right)^{\frac{\alpha}{2}} k^0}{\sqrt{\frac{D_O \pi \nu n F}{RT}}} \qquad \text{eqn.5}$$

Where F is Faradays constant, 96,485 $CMol^{-1}$, R is the gas constant, 8.314 $JK^{-1}mol^{-1}$, T is temperature, ν is the scan rate, n is the number of electrons transfer, α is the transfer coefficient, taken as 0.5 here, k^0 is the standard rate constant of electron transfer, D_O, $5.83x10^{-6}$ cm^2s^{-1}, and D_R, $6.61x10^{-6}$ cm^2s^{-1}, are the diffusion coefficients of the oxidised and reduced species, respectively in this electrolyte taken from the literature [45, 46]. For large values of Ψ the system reduced to purely reversible behaviour and for very small values of Ψ (<0.1), the system became completely irreversible. The intermediate stage between these regions with scan rate was examined in order to determine k^0.

Figure 9 shows the redox behaviour of the $Fe(CN)_6^{3-}/Fe(CN_6)^{4-}$ system during the multilayer construction of a $[BiCo]^{10-}$-based film. As can be seen with increasing layers the $Fe(CN)_6^{3-}/Fe(CN_6)^{4-}$ redox system passes from being reversible to quasi-reversible in

nature. As seen in Table 3 the k^0 value decreased from a value of 3.99 x 10^{-2} cms^{-1} to 2.27 x 10^{-3} cms^{-1}, for the bare and 6th layer, respectively. In addition the nature of the other layer, whether it was cationic or anionic, influenced the value of the k^0 obtained with higher k^0 layers being obtained when the outer layer was cationic in nature. This can be explained by the presence of repulsive interactions between the negatively charged $Fe(CN)_6^{3-}/Fe(CN_6)^{4-}$ redox system and the multilayer's outer anionic POM layer. Examining the anionic and cationic layers separately the general trend of decreasing k^0 value with increased number of layers held for both the anionic and cationic layers. The general decrease in k^0 with increasing layer number represents the increasing difficulty for potassium ferricyanide to reach the underlying electrode surface as the thickness of the film increased, hence it was taken as an indication of the film's porosity. For $[SbCo]^{10-}$-based films a similar decrease in the k^0 value was observed, depending on the cationic or anionic nature of the outer layer, as the film was constructed (Table 3), along with increased irreversible behaviour. For a six layer film, the k^0 value was approximately 1/25 of that for the initial base PDDA layer.

Figure 10 shows the behaviour of the $Fe(CN)_6^{3-}/Fe(CN_6)^{4-}$ system at a $[SbCu]^{8-}$-based films after the deposition of 2, 4 and 6 layers. As can be seen by the 4th and 6th deposited layers the $Fe(CN)_6^{3-}/Fe(CN_6)^{4-}$ system is irreversible in nature. This prevented the calculation of its k^0 value which relied on observing the transient region between reversible and irreversible regions. There was a similar dependence on the nature of the outer layer indicated for $[SbCu]^{8-}$-based films as for both $[SbCo]^{10-}$ and $[BiCo]^{10-}$-based films. There was a more dramatic decrease in the k^0 value for the $Fe(CN)_6^{3-}/Fe(CN_6)^{4-}$

system system for this $[SbCu]^{8-}$-based film than for either $[BiCo]^{10-}$- or $[SbCo]^{10-}$-based films (Table 3).

In summary, each polyoxometalate-based film formed on the working electrode surface caused a decrease in the rate of electron exchange for $Fe(CN)_6^{3-}/Fe(CN_6)^{4-}$ system at the underlying electrode. This was dependent on the cationic or anionic nature of the outer layer, with the cationic, PDDA or ruthenium metallodendrimer outerlayers displaying higher k^0 values then the anionic, polyoxometalate outerlayers. These decreases in k^0 were indicative of the increased difficulty of ferricyanide to reach the underlying electrode surface with increasing film thickness and were taken as a measure of the film's porosity. The initial k^0 values for the bare electrode differed in each case as the electrode is roughened prior to film formation, this variation in surface area leads to slightly different k^0 values for the bare electrode surfaces. Of the three films examined here, those that were formed with $[BiCo]^{10-}$ and $[SbCo]^{10-}$ exhibited similar k^0 values but films containing $[BiCo]^{10-}$ appeared slightly more porous then those with $[SbCo]^{10-}$. The behaviour observed for these films was consistent with that observed from AC impedance studies. From the literature [46] for films composed of 1,8-diisocyanooctane and Pt nanoparticles layers a decrease in k^0, by the 6^{th} layer, to $2.1x10^{-3}$ cms^{-1} was noted, or an approximate $1/20^{th}$ decrease from $41x10^{-3}$ cms^{-1}. For the polyoxometalate films examined here, $[BiCo]^{10-}$- and $[SbCo]^{10-}$-based films exhibited k^0 values approximately $1/20^{th}$ of the base electrode by their 6^{th} layer while $[SbCu]^{8-}$-based films exhibited a decrease to $1/20^{th}$ of its initial value by the 4^{th} layer.

4. Conclusions

The Layer by Layer (LBL) method was used to build reproducible multilayer assemblies composed of a series of transition metal substituted Krebs type polyoxometalates of the general formula $[X_2W_{20}M_2O_{70}(H_2O)_6]^{n-}$, X = Sb or Bi, M = Co(II) or Cu(II), n = 8^- or 10^- and a cationic ruthenium metallodendrimer $[RuDen]^{8+}$. The film's formation was due to the electrostatic attractions between the oppositely charged species. The constructed multilayer assemblies were monitored and characterized using cyclic voltammetry, AFM and AC- Impedance techniques. The assemblies exhibited pH dependent redox activity associated with the tungsten-oxo framework of each polyoxometalate with no significant redox activity for the polyoxometalate's Cu(II) centre. The reason for the latter believed to due to the ejection of the Cu(II) centre from the polyoxometalate's cage upon layer formation primarily because of the repulsive interactions between the polyoxometalate and $[RuDen]^{8+}$ moiety within the film. The tungsten – oxo redox processes of the immobilized polyoxometalates were seen to shift to negative potentials upon exposure to more alkaline pHs, this being also seen for the solution phase polyoxometalates. Scan rate studies of the multilayer films showed that the peak potentials associated with the W-O and $Ru^{II/III}$ redox couples were all independent of scan rate with the peak currents being directly proportional with scan rate up to 100mV s^{-1} for the W-O redox couples and up to 750 mVs^{-1} for the metallodendrimer's $Ru^{II/III}$ redox process. This indicates that the redox processes exhibited fast electron transfer properties characteristic for a surface controlled processes. AC impedance measurements of the polyoxometalate multilayers in the presence of the model monoelectronic redox system $Fe(CN)_6^{3-}/Fe(CN_6)^{4-}$ yielded charge transfer resistances, R_{CT}, values that increase with layer number and which are

dependant upon the nature of the multilayer's outer layer. The heterogeneous rate constant, k^o, for the $Fe(CN)_6^{3-}/Fe(CN_6)^{4-}$ system decreased with increasing layer number of the multilayer assemblies with higher values for k^o being obtained when the outer layer of each assembly was cationic in nature.

Acknowledgements

The authors would like to acknowledge research funding by the Irish Research Council for Science, Engineering and Technology (IRCSET) through the PhD Embark initiative. In addition, colleagues at Dublin City University within the School of Chemistry are acknowledged for their guidance during the AFM measurements.

References

1. G. Sigmon, J. Ling, D. Unruh, L. Moore-Shay, M. Ward, B. Weaver, P. Burns, J. Am. Chem. Soc. 131 (2009) 16648.
2. X. Lopez, C. Bo, J.M. Poblet, J. Am. Chem. Soc. 124 (2002) 12574.
3. S. Reinoso, J. Galán-Mascarós, Inorg. Chem. 49 (2010) 377.
4. B.S. Bassil, S. Nellutla, U. Kortz, A.C. Stowe, J. van tol, N.S. Dalal, B. Keita, L. Nadjo, Inorg. Chem. 44 (2005) 2659.
5. C. Li, R. Cao, K. O'Halloran, H. Ma, L. Wu, Electrochim. Acta 54 (2008) 484.
6. C. Zhang, C. Sun, S. Liu, H. Ji, Z. Su, Inorg. Chim. Acta 363 (2010) 718.
7. W. Zhao, Y. Zhang, B. Ma, Y. Ding, W. Qiu, Catal. Commun. 11 (2010) 527.
8. K.T. Venkateswara Rao, P.S.N. Rao, P. Nagaraju, P.S. Sai Prasad, N. Lingaiah, J. Mol. Catal. A: Chem 303 (2009) 84.
9. P. Liu, C. Wang, C. Li, J. Catal. 262 (2009) 159.
10. N. Antonova, J. Carbó, U. Kortz, O. Kholdeeva, J. Poblet, J. Am. Chem. Soc. 132 (2010) 7488.
11. P. Millet, R. Ngameni, S.A. Grigoriev, N. Mbemba, F. Brisset, A. Ranjbari, C. Etiévant, Int. J. Hydrogen Energy 35 (2010) 5043.
12. Y. Geletii, Z. Huang, Y. Hou, D. Musaev, T. Lian, C. Hill, J. Am. Chem. Soc. 131 (2009) 7522.
13. B. Notari, Adv. Catal. 41 (1996) 253.
14. C. Perego, A. Carati, P. Ingalina, M.A. Mantegazza, G. Bellussi, Appl. Catal., A 221 (2001) 63.

15. Loose, E. Droste, M. Bosing, H. Pohlmann, M. Dickman, C. Rosu, M. Pope, B. Krebs, Inorg. Chem, 38 (1999) 2688.

16. M. Bosing, I. Loose, H. Pohlmann, B. Krebs, Chem. Eur. J. 3 (1997).

17. J.A. Osaheni, S.A. Jenekhe, Chem. Mater. 4 (1992) 1282.

18. M.F. Roberts, S.A. Jenekhe, Chem. Mater. 6 (1994) 135.

19. M. Gerard, A. Chaubey, B.D. Malhorta, Biosensors and Bioelectronics 17 (2002) 345

20. J.F. Rusling, R.J. Forster, J. Coll. Inter. Sci. 262 (2003) 1.

21. T. McCormac, D. Farrel, D. Drennan. G. Bidan, Electroanalysis 13 (2001) 836.

22. B. Keita, L. Nadjo, J. Electroanal. Chem. 191 (1985) 441.

23. B. Keita, L. Nadjo, J. Electroanal. Chem. 354 (1993) 295.

24. B. Keita, L. Nadjo, Surf. Sci. 254 (1991) 1433.

25. B. Watson, M.A. Barteau, L. Haggerty, A.M. Lenholf, R.S. Weber, Langmuir 8 (1992) 1145.

26. B. Keita, L. Nadjo, J. Electroanal. Chem. 243 (1988) 87.

27. B. Keita, L. Nadjo, J. Electroanal. Chem. 269 (1989) 447.

28. O. Savadogo, K. Amuzgar, Int. J. Hydrogen. Energy 15 (1990) 783.

29. Z.Y. Tang, S.Q. Liu, E.K. Wang, S.J. Dong, E.B. Wang, Langmuir 16 (2000) 5806.

30. F.Z. Dahou, L. Cattin, J. Garnier, J. Ouerfelli, M. Morsli, G. Louarn, A. Bouteville, A. Khellil, J.C. Beréde, Thin Solid Films 518 (2010) 6117.

31. M. Zynek, M. Serantoni, S. Beloshapkin, E. Dempsey, T. McCormac, Electroanalysis. 19 (2007) 681.

32. L. Bi, Y. Shen, J. Jiang, E. Wang, S. Dong, Anal. Chim. Acta 534 (2005) 343.

33. K. Foster, L. Bi, T. McCormac, Electrochim. Acta 54 (2008) 868.

34. B. Haghighi, H. Hamidi, L. Gorton, Electrochim. Acta 55 (2010) 4750.

35. T. Dong, H. Ma, W. Zhang, L. Gong, F. Wang, C. Li, Adv. Colloid Interface Sci. 311 (2007) 523.

36. E. Constable, C. Housecroft, M. Cattalini, D. Phillips, New J. Chem. (1998) 193.

37. R. Neumann, Inorg. Chem. 49 (2010) 3594.

38. A. Douvas, E. Makarona, N. Glezos, P. Argitis, J. Mielczarski, E. Mielczarski, ACSnano 2 (2008) 733.

39. Li-Hua Bi, T. McCormac, S. Beloshapkinb, E. Dempsey, Electroanalysis 20 (2007) 38.

40. M. Ammam, B. Keita, L. Nadjo, I. Mbomekalle, J. Fransaer, J. Electroanal. Chem. 645 (2010) 65.

41. H. Ma, J. Peng, Z. Han, Y. Feng, E. Wang, Thin Solid Films 446 (2004) 161.

42. S. Gao, R. Cao, X. Li, Thin Solid Films 500 (2006) 283.

43. A.J. Bard, L. R. Faulkner, Electrochemical Methods: Fundamentals and Applications 2nd edition, John Wiley and Sons, Inc 2001.

44. J.J. Harris, M.L. Bruening, Langmuir 16 (2000) 2006.

45. R. Nicholson, Anal. Chem. 37 (1965) 1351.

46. S. Horwell, I. O'Neill, D. Schiffrin, J. Phys. Chem. B 107 (2003) 4844.

Figure Legends

Figure 1 (A-F). Cyclic voltammograms of the various polyoxometalates at pH 2.5 0.5 mol dm^{-3} Na_2SO_4, glassy carbon working electrode (0.0707cm^2), E vs (Ag/AgCl)/V, $1x10^{-3}$ mol dm^{-3} M of A: $[Bi_2W_{22}O_{74}(H_2O)_6]^{12-}$, B: $[Sb_2W_{22}O_{74}(OH)_2]^{12-}$, C: $[BiCo]^{10-}$ D: $[BiCu]^{8-}$ E: $[SbCo]^{10-}$ F: $[SbCu]^{8-}$, A-B: Scan rate 5 mVs^{-1}, C-F: Scan rate 10 mVs^{-1}.

Figure 2(a): Cyclic voltammograms displaying the film growth of a $[BiCo]^{10-}$-based film, on a glassy carbon working electrode (0.0707 cm^2), with an initial PDDA layer followed by alternating polyoxometalate, $[BiCo]^{10-}$, anionic and Ru(metallodendrimer) cationic layers, E vs (Ag/AgCl)/V, pH 2.0 0.5 mol dm^{-3} Na_2SO_4, scan rate 10 mVs^{-1}.

Figure 2(b): Surface coverage versus film growth for a $[BiCo]^{10-}$-based film.

Figure 3(a). Cyclic voltammograms for a film formed with an initial PDDA layer followed by alternating $[BiCo]^{10-}$ anionic and Ru(metallodendrimer) cationic layers up to six bi-layers at various electrolyte pH values. Film is formed on a glassy carbon working electrode (0.0707 cm^2), E vs (Ag/AgCl)/V, Pt counter electrode, electrolyte 0.5 mol dm^{-3} Na_2SO_4 adjusted with 0.5 mol dm^{-3} H_2SO_4 for the pH range 1.0-3.5 and 0.5 mol dm^{-3} CH_3COONa adjusted with CH_3COOH for the pH range 4.0-6.5, 10 mVs^{-1}.

Figure 3(b). pH dependence of W1 redox couple's $E_{1/2}$ for the film given in Figure 4(a).

Figure 4(a) Cyclic voltammograms for $[BiCo]^{10-}$-based films at various scan rates, Films are built on a glassy carbon working electrode (0.0707 cm^2), E vs (Ag/AgCl)/V, Pt counter electrode, electrolyte pH 2.0 0.5 mol dm^{-3} Na_2SO_4 adjusted with 0.5 mol dm^{-3} H_2SO_4, scan rates from 10-500 mVs^{-1}.

Figure 4(b). Scan rate studies for $[BiCo]^{10-}$-based film's W1 redox couple displaying current versus scan rate for two different scan rate ranges, as shown in Figure 3(a)

Figure 5 Cyclic voltammogram dislaying an example of film growth, on a glassy carbon working electrode (0.0707 cm^2), with a base PDDA layer followed by alternating polyoxometalate $[SbCu]^{8-}$ anionic and Ru(metallodendrimer) cationic layers, E vs (Ag/AgCl)/V, pH 2.0 0.5 mol dm^{-3} Na_2SO_4, scan rate 10 mVs^{-1}.

Figure 6. Cyclic voltammograms for the growth of a $[Sb_2W_{22}O_{74}(OH)_2]^{12-}$-based film, on a glassy carbon working electrode (0.0707 cm^2), with an initial PDDA layer followed by alternating $[Sb_2W_{22}O_{74}(OH)_2]^{12-}$ anionic and Ru(metallodendrimer) cationic layers, E vs (Ag/AgCl)/V, Pt counter electrode, pH 2.0 0.5 M Na_2SO_4 adjusted with 0.5 mol dm^{-3} H_2SO_4, scan rate 10mVs^{-1}.

Figure 7. AFM image of a $[SbCu]^{8-}$ based films constructed on ITO slides up to six bi-layers. AFM in contact mode, tip spring constant between 12-103N/m, tip size 3.6-5.6 mm.

Figure 8: AC impedance voltammograms for 1^{st} – 7^{th} layer, for a film containing $[BiCo]^{10-}$ as the film is constructed, 1^{st} layer: PDDA, $2^{nd}/4^{th}/6^{th}$ layer: polyoxometalate, $3^{rd}/5^{th}/7^{th}$ layer: ruthenium metallodendrimer, film formed on a glassy carbon working electrode (0.0707 cm^2), E vs (Ag/AgCl)/V, Pt counter electrode, electrolyte 0.1 mM potassium ferricyanide, 0.1 mM potassium ferrocyanide and 0.1 mol dm^{-3} KCl, applied potential 223 mV, frequency range 0.1 to $1x10^6$ Hz, voltage amplitude 5 mV.

Figure 9. Cyclic voltammograms for the redox couple of 1 mM potassium ferricyanide at electrodes modified with $[BiCo]^{10-}$-based films at 200 mVs^{-1}, after 2, 4 and 6^{th} layers, film formed on a glassy carbon working electrode (0.0707 cm^2), E vs (Ag/AgCl)/V , Pt counter electrode, electrolyte $1x10^{-3}$ mol dm^{-3} potassium ferricyanide plus 0.1 M K_2SO_4.

Figure 10. Cyclic voltammograms for the redox couple of 1 mM potassium ferricyanide at electrodes modified with $[SbCu]^{8-}$-based films at 200 mVs^{-1}, after 2, 4 and 6^{th} layers, film formed on a glassy carbon working electrode (0.0707 cm^2), E vs (Ag/AgCl)/V , Pt counter electrode, electrolyte 1 mM potassium ferricyanide plus 0.1 moldm^{-3} K_2SO_4.

Figure 1 (a-f)

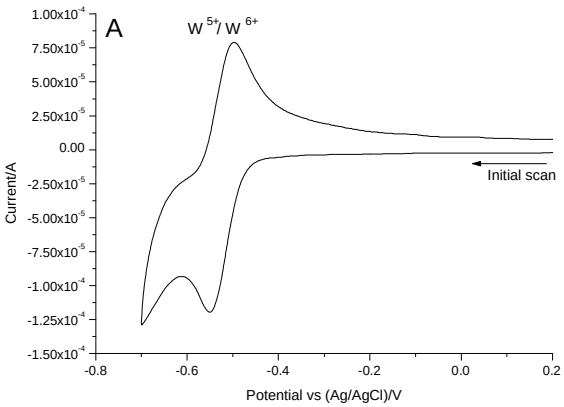
A
W 5+/ W 6+
Initial scan
Current/A
Potential vs (Ag/AgCl)/V

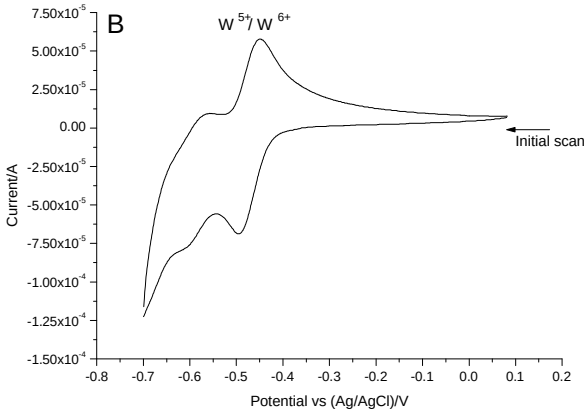
B
W 5+/ W 6+
Initial scan
Current/A
Potential vs (Ag/AgCl)/V

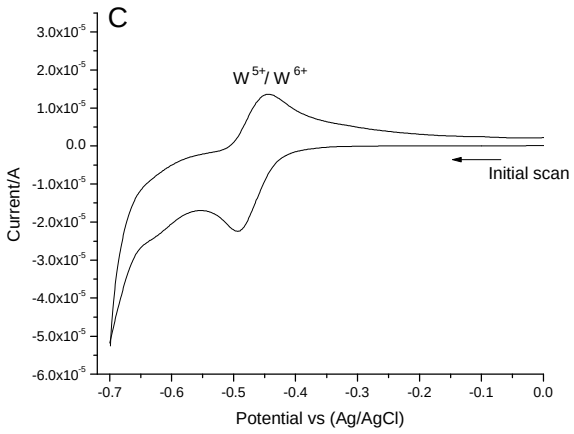
C
W5+/ W6+
Initial scan
Current/A
Potential vs (Ag/AgCl)

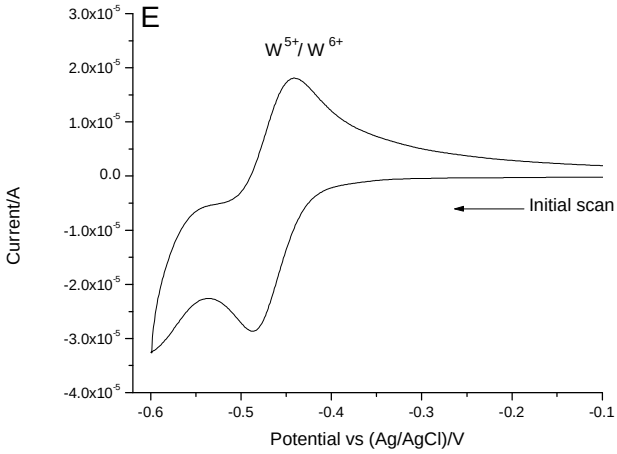
E
W5+/ W6+
Initial scan
Current/A
Potential vs (Ag/AgCl)/V

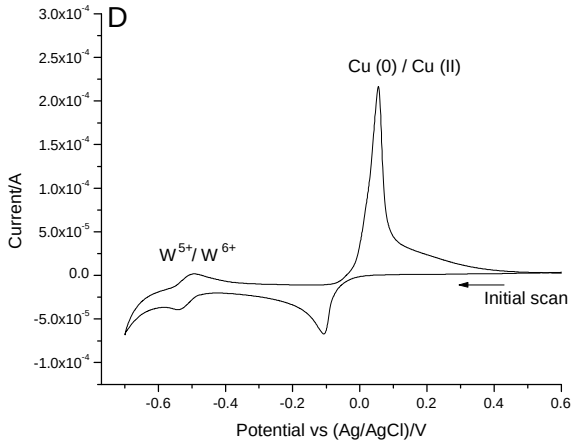
D
Cu (0) / Cu (II)
W5+/ W6+
Initial scan
Current/A
Potential vs (Ag/AgCl)/V

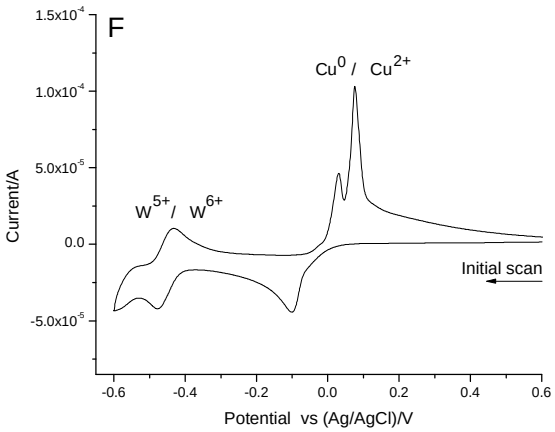
F
Cu0 / Cu2+
W5+ / W6+
Initial scan
Current/A
Potential vs (Ag/AgCl)/V

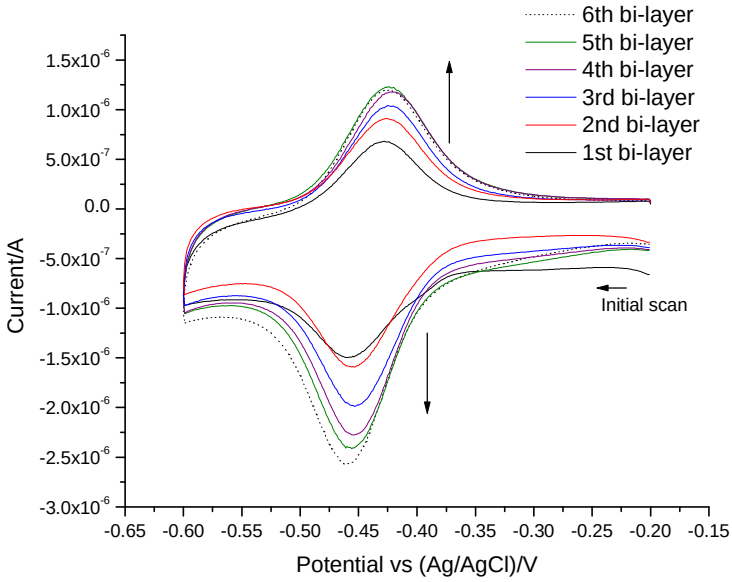

Figure 2(a).

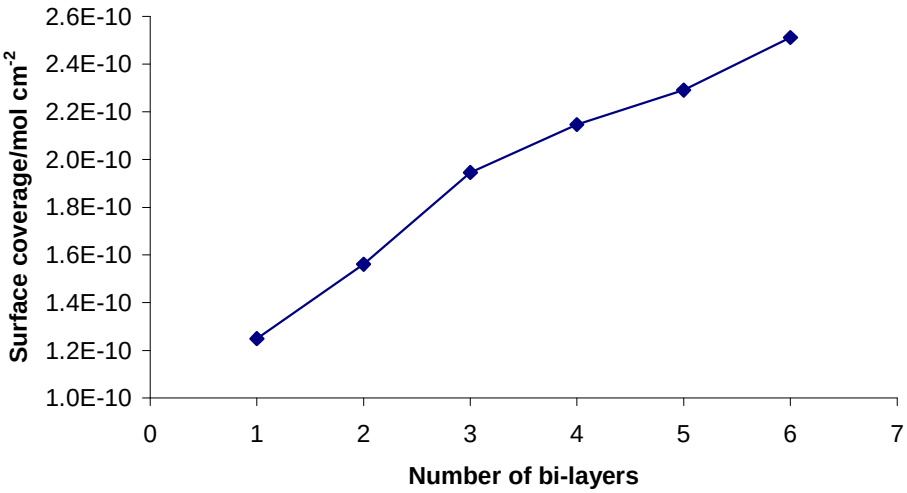

Figure 2(b).

Figure 3(a)

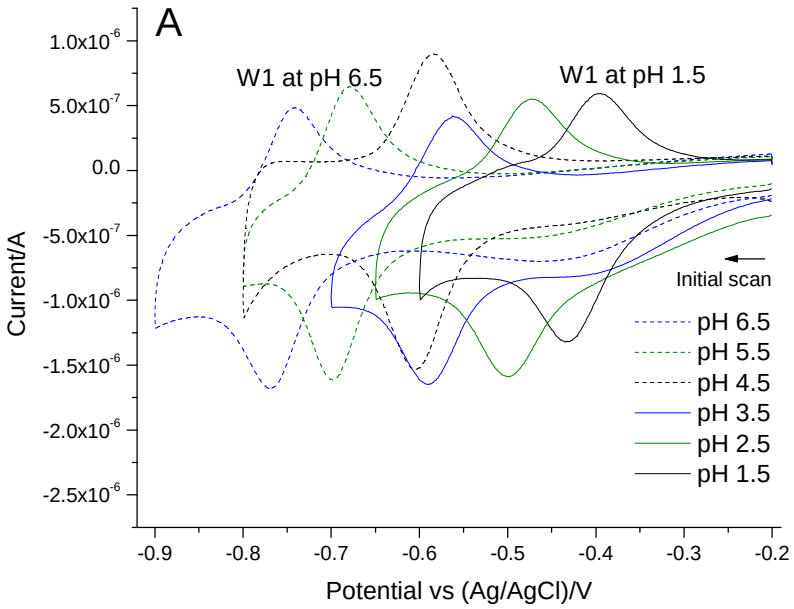

Figure 3(b)

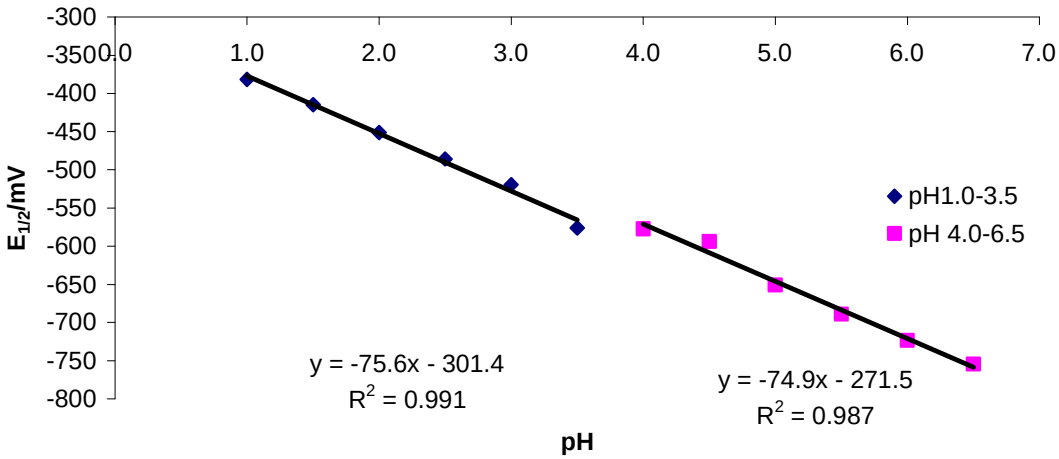

Figure 4(a)

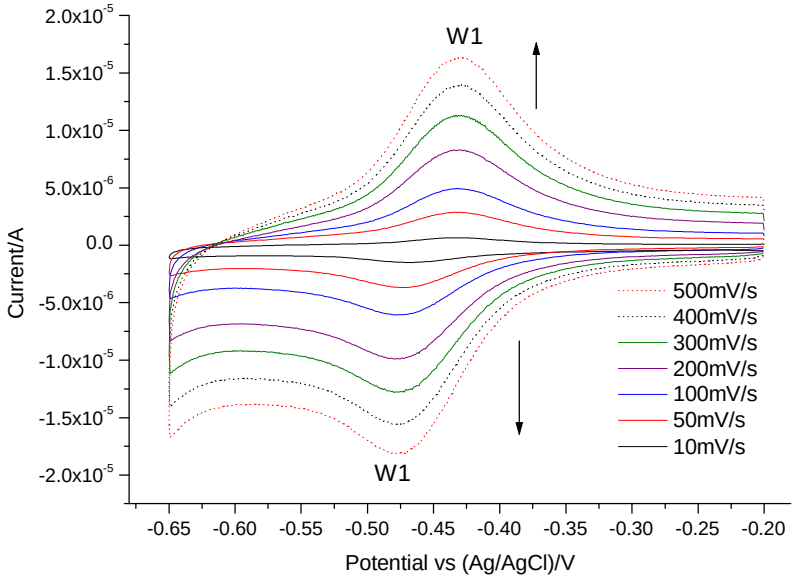

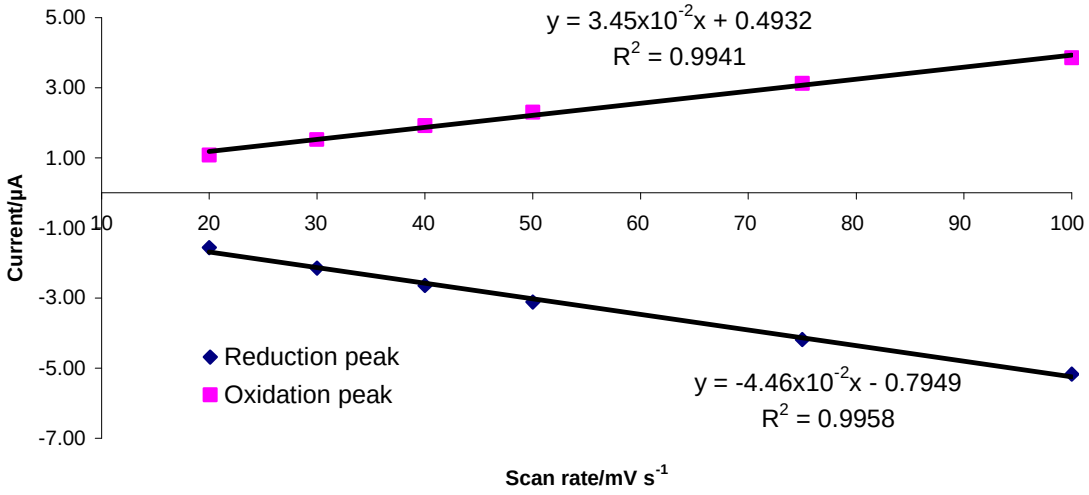

Figure 4(b)

Figure 5

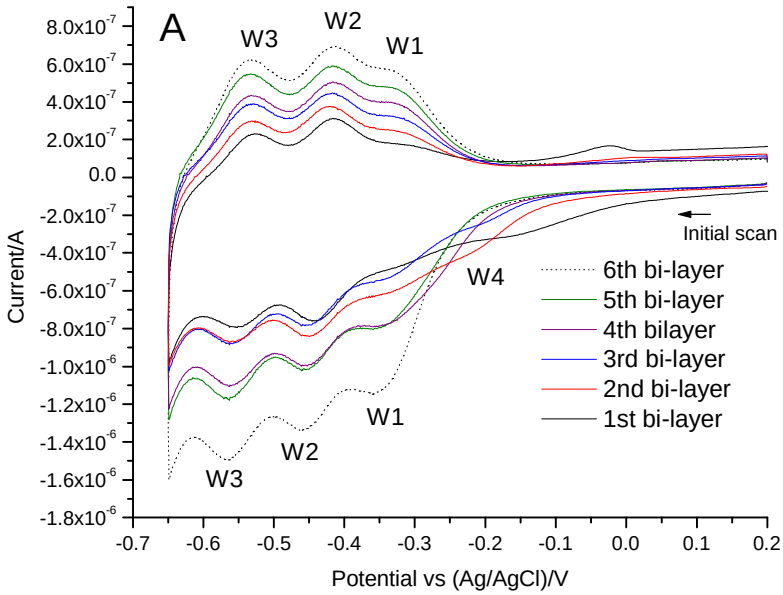
A
W3
W2
W1
W4
W1
W2
W3
Initial scan
6th bi-layer
5th bi-layer
4th bilayer
3rd bi-layer
2nd bi-layer
1st bi-layer
Current/A
Potential vs (Ag/AgCl)/V
8.0x10-7
6.0x10-7
4.0x10-7
2.0x10-7
0.0
-2.0x10-7
-4.0x10-7
-6.0x10-7
-8.0x10-7
-1.0x10-6
-1.2x10-6
-1.4x10-6
-1.6x10-6
-1.8x10-6
-0.7
-0.6
-0.5
-0.4
-0.3
-0.2
-0.1
0.0
0.1
0.2

Figure 6

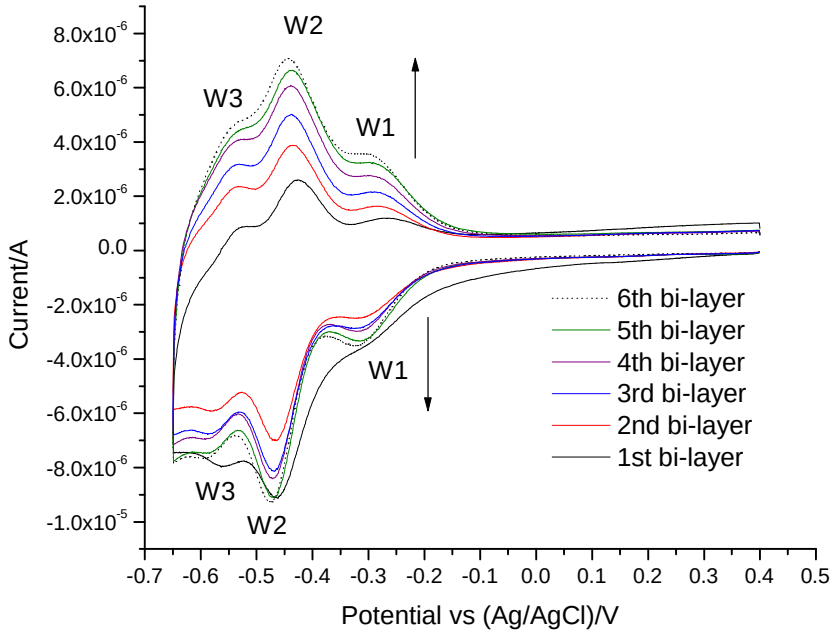
W2
W3
W1
W1
W3
W2
6th bi-layer
5th bi-layer
4th bi-layer
3rd bi-layer
2nd bi-layer
1st bi-layer
Current/A
Potential vs (Ag/AgCl)/V
8.0x10-6
6.0x10-6
4.0x10-6
2.0x10-6
0.0
-2.0x10-6
-4.0x10-6
-6.0x10-6
-8.0x10-6
-1.0x10-5
-0.7
-0.6
-0.5
-0.4
-0.3
-0.2
-0.1
0.0
0.1
0.2
0.3
0.4
0.5

Figure 7

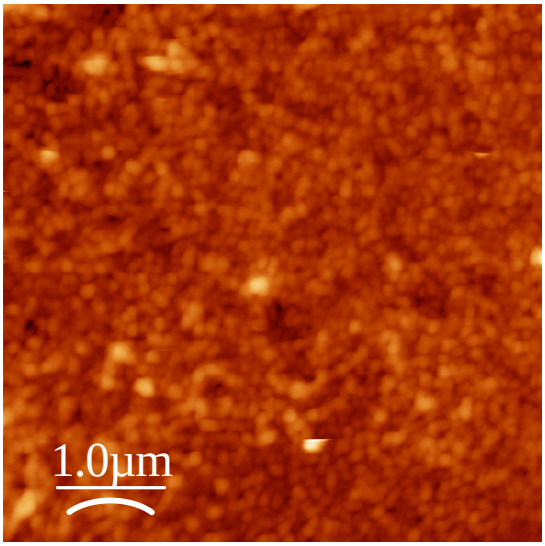

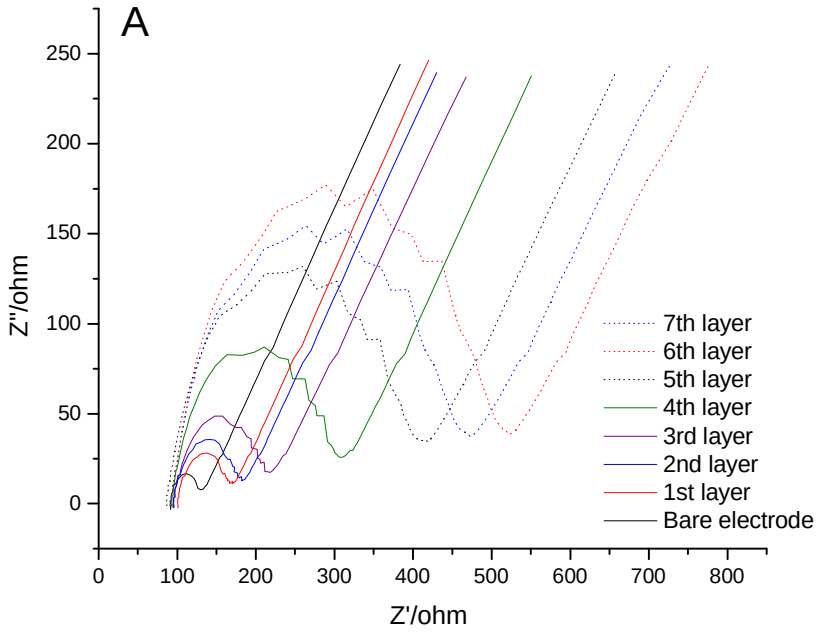
A
250
200
150
100
50
0
Z''/ohm
0
100
200
300
400
500
600
700
800
Z'/ohm
7th layer
6th layer
5th layer
4th layer
3rd layer
2nd layer
1st layer
Bare electrode

Figure 8

Figure 9

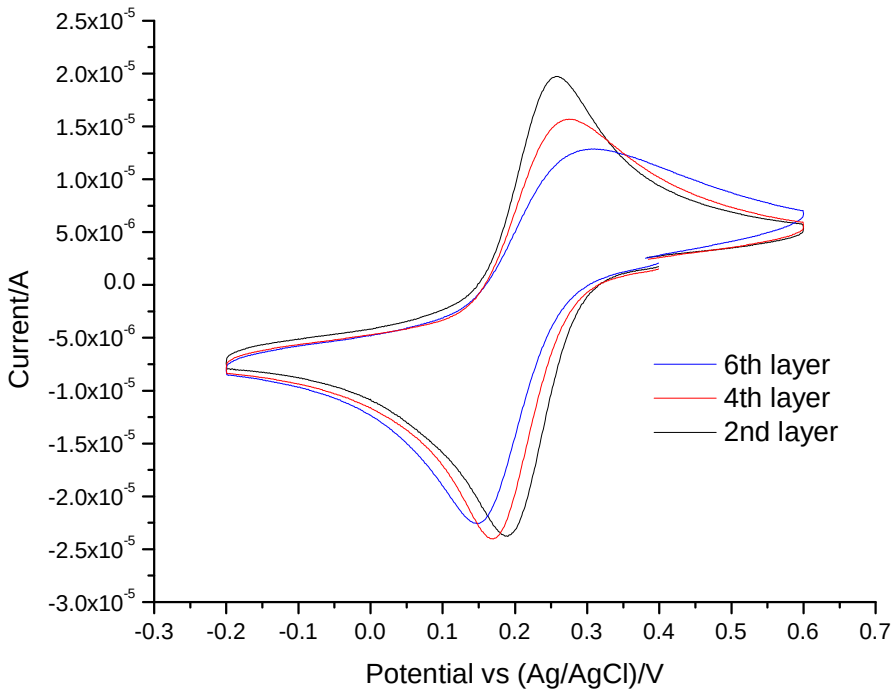
2.5x10-5
2.0x10-5
1.5x10-5
1.0x10-5
5.0x10-6
0.0
-5.0x10-6
-1.0x10-5
-1.5x10-5
-2.0x10-5
-2.5x10-5
-3.0x10-5
Current/A
-0.3
-0.2
-0.1
0.0
0.1
0.2
0.3
0.4
0.5
0.6
0.7
Potential vs (Ag/AgCl)/V
6th layer
4th layer
2nd layer

Figure 10

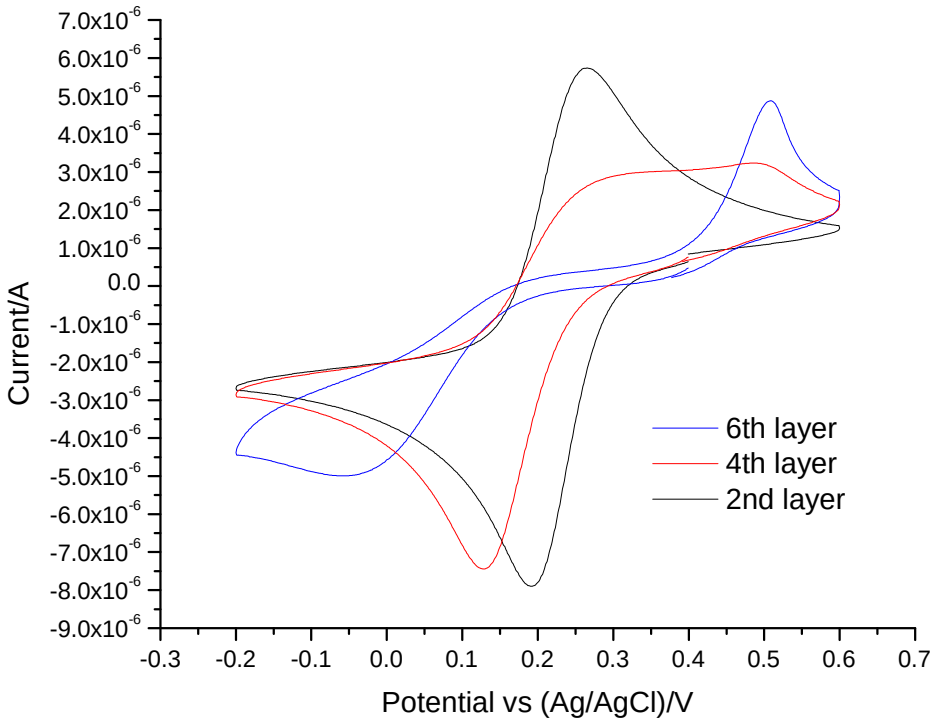
7.0x10-6
6.0x10-6
5.0x10-6
4.0x10-6
3.0x10-6
2.0x10-6
1.0x10-6
0.0
-1.0x10-6
-2.0x10-6
-3.0x10-6
-4.0x10-6
-5.0x10-6
-6.0x10-6
-7.0x10-6
-8.0x10-6
-9.0x10-6
Current/A
-0.3
-0.2
-0.1
0.0
0.1
0.2
0.3
0.4
0.5
0.6
0.7
Potential vs (Ag/AgCl)/V
6th layer
4th layer
2nd layer